Design and Analysis of a Novel Trans-inverse DC-DC Converter

Yuan, Jing; Shen, Zhan; Yang, Yongheng; Mostaan, Ali; Blaabjerg, Frede

Published in:
Proceedings of 2019 20th Workshop on Control and Modeling for Power Electronics (COMPEL)

DOI (link to publication from Publisher):
10.1109/COMPEL.2019.8769638

Publication date:
2019

Document Version
Early version, also known as pre-print

Design and Analysis of a Novel Trans-inverse DC-DC Converter

Jing Yuan[1], Zhan Shen[1], Yongheng Yang[1], Ali Mostaan[2], and Frede Blaabjerg[1]
[1]*Department of Energy Technology, Aalborg University, Denmark*
[2]*Electrical Engineering Department, University of Guilan, Iran*
Email: yua@et.aau.dk, zhs@et.aau.dk, yoy@et.aau.dk, ali_8457@yahoo.com, fbl@et.aau.dk

***Abstract*—This paper explores the coupled-inductor architectures for a trans-inverse DC-DC converter. The parasitics (e.g., leakage inductance and AC resistance) will inevitably affect the performance of the coupled-inductor and thus, the entire system. More specifically, when ignoring these parasitics, the operation principle of the DC-DC converter changes and the boosting capability is degraded. Considering the application in a trans-inverse DC-DC converter, three winding arrangements are explored in detail to demonstrate their advantages and disadvantages. Finite element analysis (FEA) on the magnetics is conducted in this paper to simulate the leakage inductance and AC resistance. Finally, the performance of the trans-inverse converter with the designed winding arrangements is verified by experimental tests.**

***Index Terms*—Coupled-inductor, finite element analysis, leakage inductance, high step-up dc-dc converter**

I. Introduction

The pollution caused by the fossil fuels is increasing with the rapid industrialization. In order to reduce the adverse impact, more environmental-friendly renewable energy services such as photovolatic (PV), wind, tide waves and fuel cells are widely used in recent years. However, the output voltage from these renewable energy resources is typically so low that they cannot be directly connected to the grid/load side. To address this, high step-up DC/DC converter become essential in many renewable energy applications [1], [2]. Although the traditional boost DC-DC converters are widely employed because of the simple structure, the low boosting ratio limits further applications in high power field. To overcome this, a variety of converters have been proposed in [3]–[16].

A high voltage gain of DC-DC converters can be achieved through various configurations, e.g., the push-pull [3], half-bridge [4], full-bridge [5] and voltage multiplier cells [6], which requires high frequency transformers. Moreover, the coupled-inductor technique is an alternative to achieve high voltage gains using less components [7], [8]. The coupled-inductors DC-DC converters based on impedance-source networks, such as Γ-source [9], improved Γ-source [10], T-source [11], trans-Z-source [12], TZ-source [13], A-source [14], Σ-source [15], and Y-source [16], provide a higher voltage gain and a wider control range compared with their counterparts. In these topologies, the voltage gain is increased with a lower turn-ratio of the coupled-inductor, which significantly contributes to the overall size reduction of the converter for higher voltage gains. However, these converters require power devices with higher voltage ratings, leading to more power losses. In addition, a lower coupled-inductor turns-ratio means that the effective duty cycle to achieve the voltage boosting is narrow in practice. That is, the converter control may be challenged due to the sensitivity of the voltage gain [17]. The trans-inverse converters can achieve high voltage gains and lower voltage stresses on the switches [17], [18]. However, these converters still operate with a limited range of duty cycles (e.g., 0-0.3). To address this, a novel trans-inverse converter was proposed in [19], where the duty cycle can vary from 0 to 1, but the large input current ripples limit its applications in PV system. To tackle the aforementioned issues, a novel trans-inverse coupled-inductor Semi-SEPIC DC-DC converter, as shown in Fig. 1, was proposed in [20] with continuous input currents and high voltage gain.

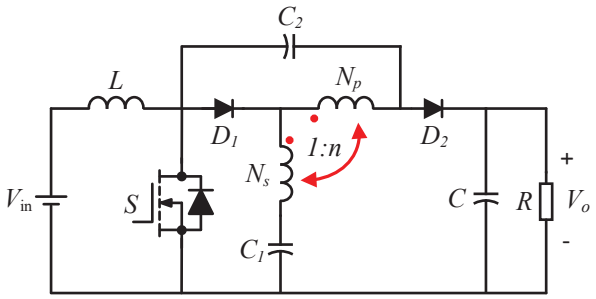

Fig. 1. Schematic of trans-inverse DC-DC converter.

It is clear that the leakage inductance will affect the performance of the trans-inverse DC-DC converter [21], as exemplified in Fig. 1. Therefore, it is necessary to achieve an optimal design of the coupled-inductors considering the effect of the leakage inductance. The accurate estimation of the coupled-inductor parasitics and the associated power losses are widely discussed in the literature [22]–[26]. Various transformer winding architectures have been explored to achieve high system efficiencies considering the leakage inductance, AC resistance and parasitic capacitance between windings. However, these solutions may not be directly applied to certain trans-inverse converters, where more attempts should be made.

In this paper, the coupled-inductor for the trans-inverse DC-DC converter (see Fig. 1) is thus analyzed and designed to minimize the leakage inductance. The rest of this paper is organized as follows. In Section II, the operation principle of the trans-inverse DC-DC topology is presented. Moreover, how the leakage inductance affects the operation principle is discussed. In Section III, the parasitics of the coupled-inductor

978-1-7281-1842-0/19/$31.00 © 2019 IEEE

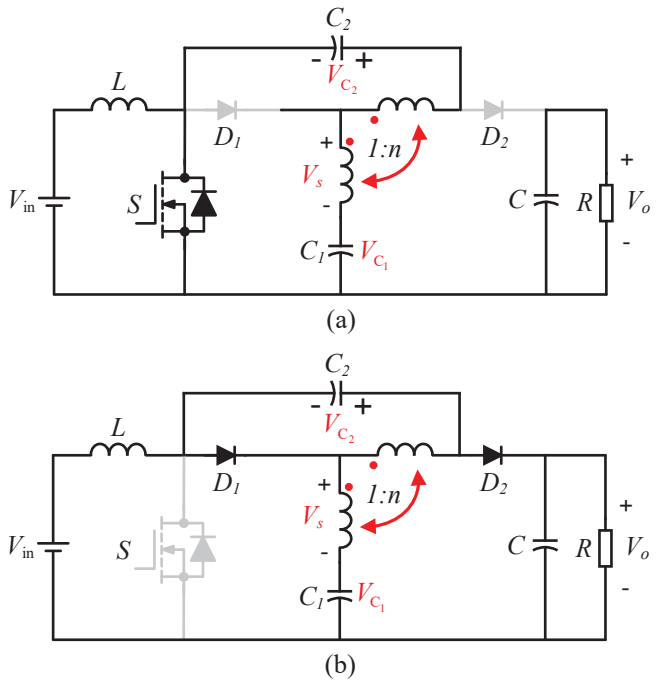

Fig. 2. Equivalent circuits of the trans-inverse converter when the switch is turned (a) ON and (b) OFF.

with three different winding architectures are explored by finite element analysis (FEA) simulations in ANSYS Maxwell. The experimental tests are given in Section IV, which verify the performance of the designed coupled-inductors. Finally, the paper concludes in Section V.

II. Operation Principle of the Trans-inverse Converter

The equivalent circuits of the trans-inverse semi-SEPIC DC/DC converter [20] are presented in Fig. 2, which includes of an input inductor (L), one active switch (S), three capacitors (C_1, C_2, C), two diodes (D_1, D_2), a leakage inductance (L_m) and a coupled inductor, where $n = N_p/N_s$ represents the turn ratio. There are two states in one switching cycle, as shown in Fig. 2. When the switch is turned ON (see Fig. 2(a)), both diodes are reverse-biased and the input source charges the input inductor L. Moreover, the source cannot transfer power to the load R due to the reverse-biased D_2, but it is powered by the output capacitor C. According to Fig. 2(a), it can be obtained that:

$$V_s = \frac{V_{C_1} - V_{C_2}}{n-1} \tag{1}$$

with V_s being the voltage across the secondary side inductance, V_{C_1} and V_{C_2} being the voltage across the capacitors C_1 and C_2.

When the switch is turned OFF and both diodes will be in the OFF state, as shown in Fig. 2(b). The stored energy in the input inductor can be delivered to the load. In this case, the voltage across the leakage inductance can be given as

$$V_s = \frac{V_{C_1} - V_o}{n-1} \tag{2}$$

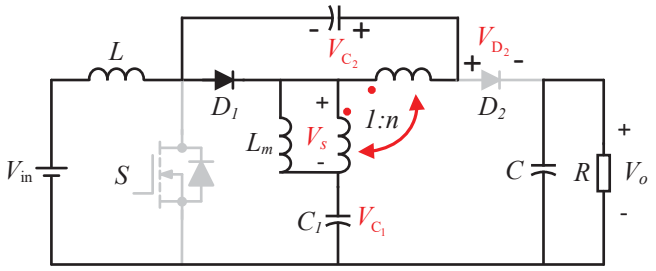

Fig. 3. : Equivalent circuit of the trans-inverse converter when the diode D_2 is turned off. (L_m is the leakage inductance)

in which V_o is the output voltage. By applying the volt-second balance principle, the voltages across C_1 and C_2, and the output voltages are obtained as

$$V_{C_1} = \left(1 + \frac{nD/(n-1)}{1-D}\right) V_{\text{in}} \tag{3}$$

$$V_{C_2} = \left(\frac{nD/(n-1)}{1-D}\right) V_{\text{in}} \tag{4}$$

$$V_o = G \cdot V_{\text{in}} = \left(\frac{1 + nD/(n-1)}{1-D}\right) V_{\text{in}} \tag{5}$$

where G is the voltage gain and D is the duty cycle.

The above analysis has been done with the assumption that the effect of the leakage inductance is neglected. If the leakage inductance is considered, the equivalent circuit for the trans-inverse converter is as shown in Fig. 3, where D_2 is turned OFF, and S is in the OFF state. The effect of the leakage inductance on the diode (D_2) voltage is shown in Fig. 4. It is observed in Fig. 4 that the voltage of D_2 has changed compared with the condition without the leakage inductance. Moreover, the boosting capability will also be degraded due to the effect of the leakage inductance. Thus, it is necessary to minimize the effect of the leakage inductance through properly designing the coupled-inductor for the trans-inverse converter.

III. Finite Element Analysis

Three winding arrangements (P/S, S/P/S, and PS/SP/S) are explored in this paper, as shown in Fig. 5, where P and S represent the primary and secondary windings with a turn ratio of 20:28. The model of the core is ETD 59/31/22/N87. The winding configurations are summarized in Table I.

In winding W_1, there is one layer with 20 turns on the primary side and two layers with 20 turns and 8 turns on the secondary side, as shown in Fig. 5(a). Moreover, for the winding W_2 in Fig. 5(b), it employs an interleaved structure, where the single primary layer is located between the two secondary layers side. A more complicated interleaved structure, as shown in Fig. 5(c) is applied in the winding W_3, where the primary and secondary windings are distributed equally in the first and second layer. The magnetomotive force (MMF) distributions for the three windings are shown in Fig. 6.

Fig. 7 shows a close-up of the magnetic field energy of the three investigated winding structures. Between the primary and secondary windings in Fig. 7(a) and (b), the magnetic

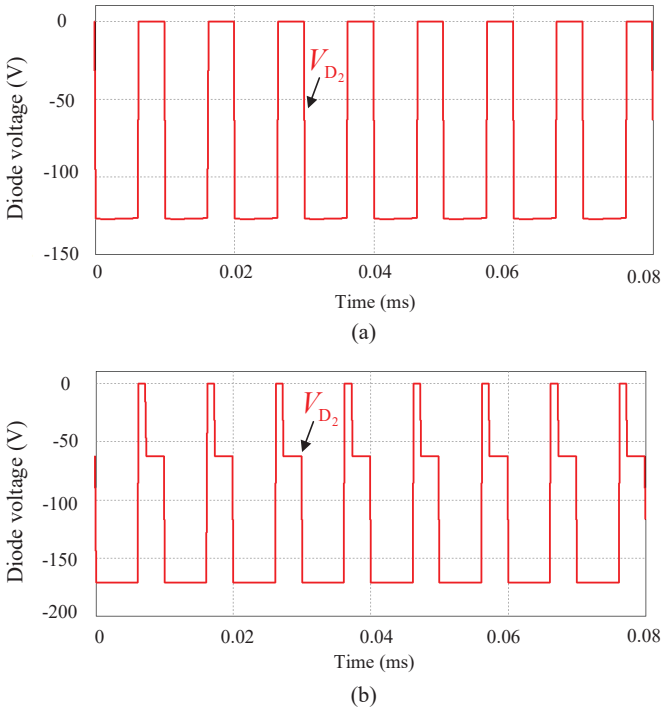

Fig. 4. Diode voltage of D_2 for the trans-inverse converter : (a) without, and (b) with the leakage inductance effect.

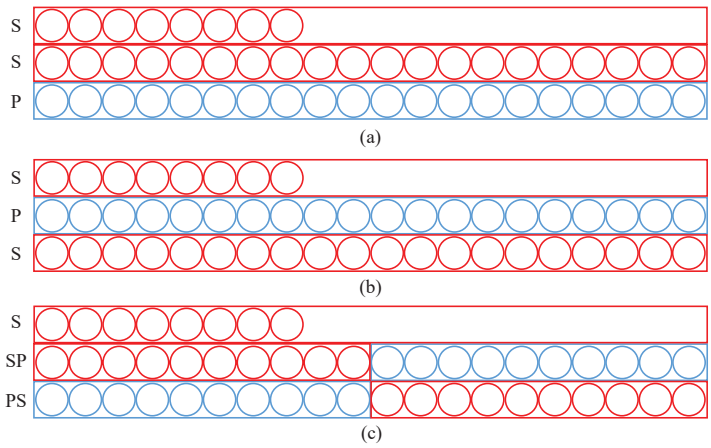

Fig. 5. Winding arrangement: (a) non-interleaved(S/P), (b) partially interleaved, and (c) fully-interleaved (PS/SP/S).

TABLE I
COUPLED-INDUCTOR ARCHITECTURES.

Design	Build-up	Primary layer and turn	Secondary layer and turn
W_1	P/S	1 and 20	2 and 20/8
W_2	S/P/S	1 and 20	2 and 20/8
W_3	PS/SP/S	2 and 10/10	3 and 10/10/8

energy is the highest in the space. In the non-interleaved winding arrangement, the MMF is the highest among all the solutions, more energy is stored between the primary and secondary windings, compared with the interleaved structures.

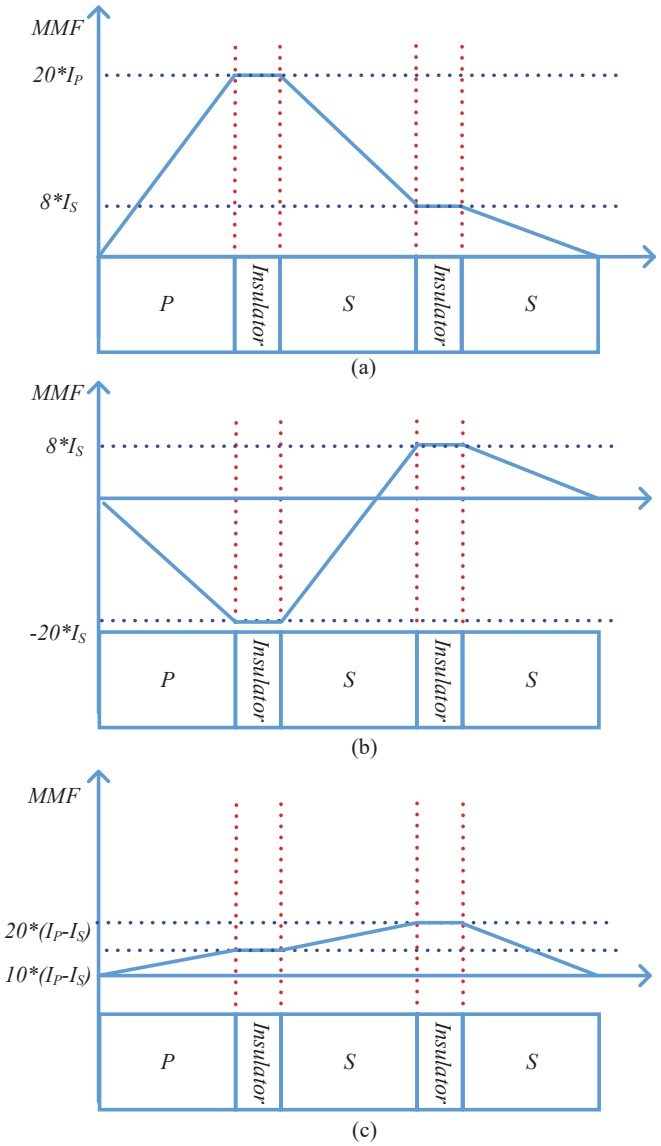

Fig. 6. Magnetomotive force (MMF) distribution for the three coupled-inductor arrangements: (a) winding W_1 (P/S), and (b) winding W_2 (S/P/S), and (c) winding W_3 (PS/SP/S).

That means, a higher leakage inductance is achieved in the non-interleaved arrangements. In the interleaved solutions, the latter is more interleaved because the primary winding is split up into two parts. More fabrication cost can be expected in this solution, as shown in Fig. 7(c). However, the highest MMF of both Fig. 7(b) and (c) are identical. However, the average MMF in Fig. 7(b) is larger than that in Fig. 7(c), which results in a higher AC resistance and leakage inductance than Fig. 7(c). In addition, the facing area between the primary and secondary in Fig. 7(b) and (c) is very close, and therefore, their stray capacitance difference is expected to be minor. This is also verified in the simulation results in Fig. 7(c) and Fig. 8(a), and it is concluded in Table II. Therefore, a “more” interleaved structure guarantees lower leakage inductance and AC losses. The trade-off between the leakage inductance and AC resistance

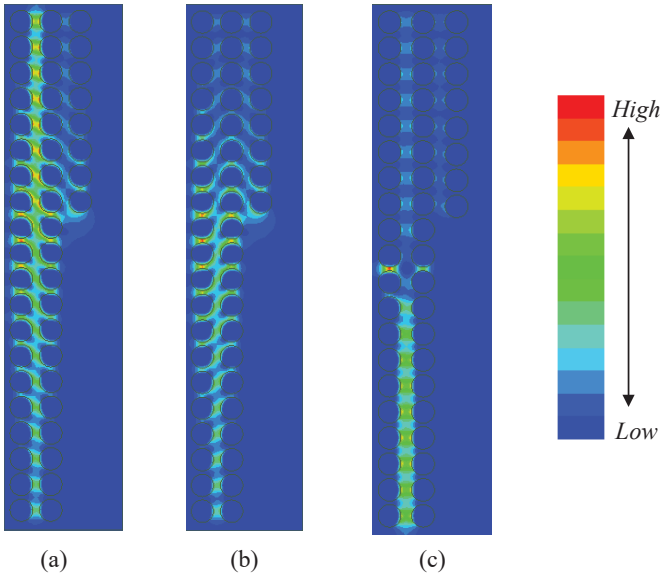

Fig. 7. Simulation plots of energy: (a) non-interleaved(P/S), (b) partially interleaved (S/P/S), and (c) fully-interleaved (PS/SP/S).

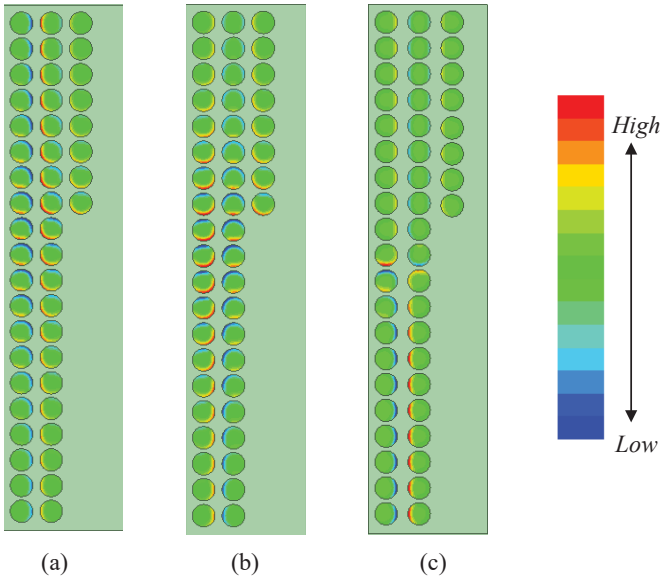

Fig. 8. Simulation plots of AC current density: (a) non-interleaved(P/S), (b) partially interleaved (S/P/S), and (c) fully-interleaved (PS/SP/S).

is further analyzed in the following.

The switching frequency of the trans-inverse converter is 100 kHz, and thus the AC resistance is simulated at 100 kHz for the three winding configurations. The current density for three winding buildups are shown in Fig. 8. Both the leakage inductance and AC resistance are calculated with the leakage magnetic field. It can be observed in Fig. 6 that the maximum MMF in the interleaved architecture is much lower than that in the non-interleaved one. Hence, the current density in the interleaved buildups (e.g., Figs. 8(b) and Fig. 8(c)) are much lower and more evenly distributed compared with the non-interleaved buildup (e.g., Fig. 8(a)). As a consequence, lower AC resistance can be achieved. Furthermore, due to the asymmetrical distribution of the winding for both primary and secondary winding, the "two-dimensional effect" appears in all the cases, where the field distortion along the horizontal direction caucuses additional resistance losses in the magnetics. Due to the more effective mixture of the primary and secondary windings, this field distortion in Fig. 8(c) is not as severe as that in Fig. 8(a) and (b). Therefore, the current density in Fig. 8(c) is distributed along the magnetic field in the vertical direction, compared with Fig. 8(a) and Fig. 8(b) with a horizontal direction component. It also decreases the AC resistance in Fig. 8(c) as well.

IV. Experimental Verification

In order to verify the above analysis, experimental tests are performed having three windings. The input voltage is 48 V and the duty cycle is set to 0.62. Based on (5), the boosted voltage should be 400 V. The parameters of the setup is shown in Table II. Furthermore, three coupled-inductors are measured, and the comparisons are shown in Table III. It can be observed in Table III that the winding W_3 has the smallest leakage inductance and ac resistance compared with the other two structures.

TABLE II
Design Parameters of the Proposed Converter.

Parameter/Decription	Value/Part Number
Power rating	150-400 W
Input/Output voltage	48/400 V
Capacitor/input inductance	100 μF/640 μH
Turn ratio	28:20 Core:B66397G0000X197
Switching frequency	100 kHz
Duty Cycle	0.62
Switch S	IPP60R099C6XKSA1
Diode D1&D2	IDP30E65D2XKSA1

TABLE III
Parameters Comparison.

	Leakage inductance		AC resistance	
	Simulation value	Measured value	Simulation value	Measured value
W_1	2.47 μH	4.3 μH	0.23 Ω	0.27 Ω
W_2	1.91 μH	3.33 μH	0.13 Ω	0.157 Ω
W_3	1.29 μH	1.8 μH	0.06 Ω	0.1 Ω

In order to verify the performance of the three windings in the trans-inverse converter, experimental tests are further carried out on a trans-inverse converter. The experimental results are shown in Fig. 9. It can be seen in Fig. 9 that the output voltages in the three windings are 366 V, 385 V and 395 V, where the winding W_3 has the best boosting capability due to its low leakage inductance and AC resistance. Moreover, it can be seen in Fig. 9 that in the windings W_1 and W_2, the diode voltage is different from that of the winding W_3, which is in agreement with the results in Fig. 4.

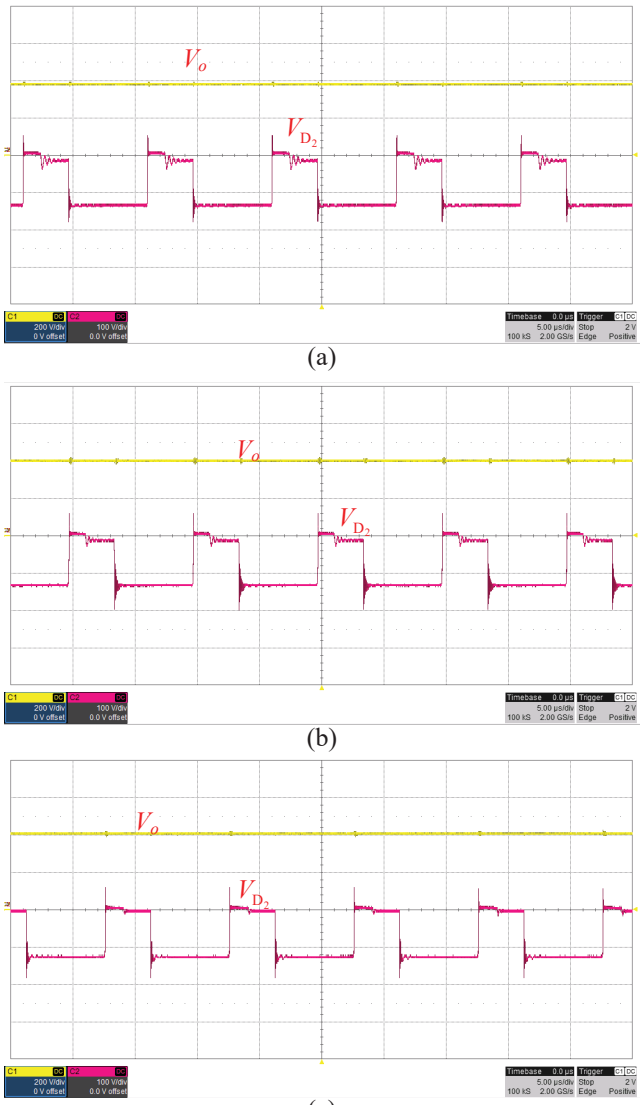

Fig. 9. Experimental results by using (a) winding W_1 (P/S), and (b) winding W_2 (S/P/S), and (c) winding W_3 (PS/SP/S) (Ouput voltage V_o (200 V/div) and Capacitor voltage V_{D_2} (100 V/div)).

V. Conclusion

In this paper, the coupled inductor architectures for a novel trans-inverse DC-DC converter were explored. It has been revealed that the performance of the trans-inverse DC-DC converter is affected by the coupled-inductor parameters. In order to optimize the design of the coupled-inductor, three winding buildups were presented. The simulation results using the FEA in ANSYS have verified that the interleaved buildups have superior performance in terms of low leakage inductance and small AC resistance. Finally, the experimental results have verified the theoretical analysis.

References

[1] W. Li and X. He, "Review of nonisolated high-step-up DC/DC converters in photovoltaic grid-connected applications," *IEEE Trans. Ind. Electron.*, vol. 58, no. 4, pp. 1239–1250, Apr. 2011.

[2] F. Blaabjerg, C. Chen, and S. B. Kjaer, "Power electronics as efficient interface in dispersed power generation systems," *IEEE Trans Power Electron*, vol. 19, no. 5, pp. 1184–1194, Sep. 2004.

[3] S. Li, K. Xiangli, and K. M. Smedley, "A control map for a bidirectional PWM plus phase-shift-modulated pushpull DCDC converter," *IEEE Trans. Ind. Electron.*, vol. 64, no. 11, pp. 8514–8524, Nov. 2017.

[4] K. Xiangli, S. Li, and K. M. Smedley, "Decoupled pwm plus phase-shift control for a dual-half-bridge bidirectional DC-DC converter," *IEEE Trans. Power Electron.*, vol. 33, no. 8, pp. 7203–7213, Aug. 2018.

[5] A. J. B. Bottion and I. Barbi, "Input-series and output-series connected modular output capacitor full-bridge pwm DC-DC converter," *IEEE Trans. Ind. Electron.*, vol. 62, no. 10, pp. 6213–6221, Oct. 2015.

[6] B. P. Baddipadiga and M. Ferdowsi, "A high-voltage-gain dc-dc converter based on modified dickson charge pump voltage multiplier," *IEEE Trans. Power Electron.*, vol. 32, no. 10, pp. 7707–7715, Oct. 2017.

[7] J. Yao, A. Abramovitz, and K. M. Smedley, "Analysis and design of charge pump-assisted high step-up tapped inductor SEPIC converter with an inductorless regenerative snubber," *IEEE Trans. Power Electron.*, vol. 30, no. 10, pp. 5565–5580, Oct. 2015.

[8] K. Tseng, J. Lin, and C. Huang, "High step-up converter with three-winding coupled inductor for fuel cell energy source applications," *IEEE Trans. Power Electron.*, vol. 30, no. 2, pp. 574–581, Feb. 2015.

[9] P. C. Loh, D. Li, and F. Blaabjerg, "Γ-Z-source inverters," *IEEE Trans. Power Electron.*, vol. 28, no. 11, pp. 4880–4884, Nov. 2013.

[10] W. Mo, P. C. Loh, and F. Blaabjerg, "Asymmetrical Γ-source inverters," *IEEE Trans. Ind. Electron.*, vol. 61, no. 2, pp. 637–647, Feb. 2014.

[11] R. Strzelecki, M. Adamowicz, N. Strzelecka, and W. Bury, "New type t-source inverter," in *Proc. 2009 CPE*, May 2009, pp. 191–195.

[12] W. Qian, F. Z. Peng, and H. Cha, "Trans-Z-source inverters," *IEEE Trans. Power Electron.*, vol. 26, no. 12, pp. 3453–3463, Dec. 2011.

[13] M. Nguyen, Y. Lim, and Y. Kim, "TZ-source inverters," *IEEE Trans. Ind. Electron.*, vol. 60, no. 12, pp. 5686–5695, Dec. 2013.

[14] Y. P. Siwakoti, F. Blaabjerg, V. P. Galigekere, A. Ayachit, and M. K. Kazimierczuk, "A-source impedance network," *IEEE Trans. Power Electron.*, vol. 31, no. 12, pp. 8081–8087, Dec. 2016.

[15] J. J. Soon and K. Low, "Sigma-z-source inverters," *IET Power Electron.*, vol. 8, no. 5, pp. 715–723, 2015.

[16] Y. P. Siwakoti, P. C. Loh, F. Blaabjerg, S. J. Andreasen, and G. E. Town, "Y-source boost DC/DC converter for distributed generation," *IEEE Trans. Ind. Electron.*, vol. 62, no. 2, pp. 1059–1069, Feb. 2015.

[17] Y. P. Siwakoti, F. Blaabjerg, and P. Chiang Loh, "High step-up trans-inverse (Tx^{-1}) DC-DC converter for the distributed generation system," *IEEE Trans. Ind. Electron.*, vol. 63, no. 7, pp. 4278–4291, Jul. 2016.

[18] H. Liu, J. Wang, and Y. Ji, "A novel high step-up coupled-inductor DC-DC converter with reduced power device voltage stress," *IEEE J. Emerg. Sel. Top. Power Electron.*, pp. 1–1, 2018, doi: 10.1109/JESTPE.2018.2868769.

[19] H. Liu, F. Li, and P. Wheeler, "A family of DC-DC converters deduced from impedance source DC-DC converters for high step-up conversion," *IEEE Trans. Ind. Electron.*, vol. 63, no. 11, pp. 6856–6866, Nov. 2016.

[20] A. Mostaan, J. Yuan, Y. Siwakoti, S. Esmaeili, and F. Blaabjerg, "A trans-inverse coupled-inductor semi SEPIC DC/DC converter with full control range," *IEEE Trans. Power Electron.*, pp. 1–1, 2019, doi: 10.1109/TPEL.2019.2917306.

[21] Y. P. Siwakoti, P. C. Loh, F. Blaabjerg, and G. E. Town, "Effects of leakage inductances on magnetically coupled Y-source network," *IEEE Trans. Power Electron.*, vol. 29, no. 11, pp. 5662–5666, Nov. 2014.

[22] Z. Ouyang, O. C. Thomsen, and M. A. E. Andersen, "Optimal design and tradeoff analysis of planar transformer in high-power DC-DC converters," *IEEE Trans. Ind. Electron.*, vol. 59, no. 7, pp. 2800–2810, Jul. 2012.

[23] P. Thummala, H. Schneider, Z. Zhang, and M. A. E. Andersen, "Investigation of transformer winding architectures for high-voltage (2.5 kV) capacitor charging and discharging applications," *IEEE Trans. Power Electron.*, vol. 31, no. 8, pp. 5786–5796, Aug. 2016.

[24] Z. Ouyang, J. Zhang, and W. G. Hurley, "Calculation of leakage inductance for high-frequency transformers," *IEEE Trans. Power Electron.*, vol. 30, no. 10, pp. 5769–5775, Oct. 2015.

[25] J. Biela and J. W. Kolar, "Using transformer parasitics for resonant converters a review of the calculation of the stray capacitance of transformers," *IEEE Trans. Ind. Appl.*, vol. 44, no. 1, pp. 223–233, Jan. 2008.

[26] Z. Shen, H. Wang, Y. Shen, Z. Qin, and F. Blaabjerg, "An improved stray capacitance model for inductors," *IEEE Trans. Power Electron.*, pp. 1–1, 2019, doi: 10.1109/TPEL.2019.2897787.